



Microstructural Analysis and Integrity of Drilling Surfaces on Titanium Alloy (Ti–6Al–4V) Using Heat-Sink-Based Cryogenic Cooling

Dipesh B. Trivedi¹ · Milind D. Atrey¹ · Suhas S. Joshi²

Received: 14 May 2023 / Revised: 18 August 2023 / Accepted: 3 September 2023 / Published online: 26 September 2023
© ASM International 2023

Abstract

Low thermal conductivity of titanium alloy tends to increase the cutting temperature and tool wear, which can thereafter adversely affect the integrity of machined surfaces. Therefore, EBSD was performed dry and various cryogenic chilling procedures to characterize the microstructure and mechanical properties of the drilled surfaces on the titanium alloy. The heat-sink channel was used during drilling for effective heat dissipation by flowing the cryogenic coolant through it. Dry and heat-sink-based cryogenic cooling was used for drilling trials, with cutting speeds of 65 m/min and 95 m/min, feed rates of 0.1 mm/rev and 0.2 mm/rev, and cryogenic temperatures of $-25\text{ }^{\circ}\text{C}$, $-50\text{ }^{\circ}\text{C}$ and $-75\text{ }^{\circ}\text{C}$. A whole indexing of the grain structure was observed under the drilling edge using cryogenic cooling with a heat-sink. The cryogenic cooling also gave the smallest machining affected zone of $6\text{ }\mu\text{m}$, and the strain in the grain of 0.4 and 1.1 at the feed rate of 0.1 mm/rev and 0.2 mm/rev, respectively, resulted in the uppermost standardized image quality value which denotes the highest defect-free microstructure on the drilled surfaces, the least value of low-angle boundaries of grains and kernel average misorientation and a higher value of nano-hardness of 8 GPa as compared to dry drilling.

Keywords Titanium drilling · Heat-sink-based cryogenic cooling · Scanning electron microscopy (SEM) · Electron backscattered diffraction (EBSD) · Surface integrity

Introduction

Machined surface integrity plays a key role in manufacturing of aerospace parts because it affects functional performance, reliability and service of components being manufactured. Microstructural assessment, surface topography, hardness and induced stresses are the most affecting factors to determine functionality and reliability of machine component [1]. Therefore, analysis of machined surface integrity on Ti–6Al–4V in various manufacturing processes is a current challenging area of research.

Liquid nitrogen (LN_2) is a well-known cryogenic coolant in various metal cutting processes as it is safe to environment and non-toxic [2]. Hong et al. found cryogenic coolant as in metal cutting operations effective for removing heat from

the cutting zones, lowering the cutting temperature, altering frictional properties at the chip-tool interface region, and helping modify tool and work material properties [3]. In machining of titanium alloys, researchers have examined machined surface integrity using cryogenic coolant in different ways.

Joshi et al. [4] analyzed microstructure of machined surfaces on titanium alloys. They observed a bigger deepness of machining affected zone on α and $(\alpha + \beta)$ alloy than on β -rich alloy, which could be due to coarser grain size in the former. Comparatively, a reduced machining affected region was observed on β -rich alloy due to the finer grain size, and lamellar microstructure in these titanium alloys. Telrandhe et al. [5] while understanding changes in microstructure on the machined surfaces on Ti–6Al–4V showed that dissimilar grain size and misorientations occur in the surfaces due to a variation in the annealing temperatures. Due to the large size of grains, deformation twins were observed that appeared helpful in reducing cutting forces at higher speeds. Further, Telrandhe et al. [6] while studying the effect of laser heat treatment on machinability of Ti–6Al–4V observed compression twins at the grain boundary and tensile twins along

✉ Suhas S. Joshi
ssjoshi@iitb.ac.in; director@iiti.ac.in

¹ Department of Mechanical Engineering, Indian Institute of Technology Bombay, Mumbai 400076, India

² Department of Mechanical Engineering, Indian Institute of Technology Indore, Indore 453552, India

the machined sub-surfaces. Wang et al. [7] analyzed mechanism of nanoscale twins induced by plastic deformation in high-speed machining of Ti–6Al–4V. It was determined by them that slip deformation occurs at the lower cutting speed, whereas twins occur at the higher cutting speed due to high rate of stress and strain. Gu et al. [8] experimentally investigated the effect of cryogenic cooling and aging on twin formation in Ti–6Al–4V alloy. After cryogenic treatment, dislocations density increased and twins occur in the microstructure, which further increase due to aging treatment. Choi et al. [9] deformed titanium at room temperature as well as cryogenic temperatures and compared twin deformation and the twin structure developed. A higher twinning deformation was found at temperature of 77 K than at 293 K during rolling of titanium alloy. Further, the grain structure gets refined due to twin formation at the cryogenic temperature. Weng et al. [10] studied microstructure and wear characteristics of titanium alloy under room temperature and a fixed cryogenic temperature at $-172\text{ }^{\circ}\text{C}$. Higher dislocations were found in the grain boundaries of α -phase near surface microstructure of Ti–6Al–4V. Further, α and β phase grains were refined under cryogenic cooling conditions. Near the surfaces and beneath of titanium samples, comparatively little plastic distortion was observed under cryogenic cooling, whereas the deformation was severe under room temperature condition. Birmingham et al. [11] performed cryogenic machining experimentation on Ti–6Al–4V to check its effect on surface integrity. It was evident from microstructure analysis that cryogenic cooling reduces heat from the cutting zone and restricts heat transfer to the tool by decreasing the contact length between tool and chip. Thus, tool life increased which resulted in improvement in surface integrity. Further, it is found from the literature that application of cryogenic coolant enhances twin formation in titanium alloy.

Gupta et al. [12] experimentally characterized performance of cryogenic MQL in turning Ti–6Al–4V. Their result revealed that cryogenic cooling offers higher hardness to the machined surfaces than due to other cooling techniques. Percin et al. [13] performed micro-drilling experiments on Ti–6Al–4V to understand the effect of different cooling conditions, such as dry, flood, MQL and cryogenic cooling on micro-hardness. Sub-surface micro-hardness obtained under cryogenic cooling conditions showed the highest value as compared to other cooling conditions. Dinesh et al. [14] checked surface quality of ZK 60 MG alloy in cryogenic turning experiments and compared results with dry cutting. Under low temperature in cryogenic cooling, the work material becomes harder as the liquid nitrogen extracts heat generated from machined surfaces which increases its hardness over that of in dry cutting.

Shukla et al. [15] studied the effect of cryogenic rapid cooling on microstructure and micro-hardness of titanium alloy. These results were compared with other quenching

media, such as water and air with different heat treatment processes. Minimum micro-hardness and lowest percentage of grain boundary region were observed under cryogenic quenching with annealed titanium samples, whereas the maximum micro-hardness was evident under cryogenic quenching with solution-treated titanium samples. The reason behind this occurrence is due to an increase of bimodal α , β grains and α – β interfaces. Won et al. [16] deformed pure titanium using liquid nitrogen at 77 K. They found separate twins in the grains which results into twinning-induced grain refinement. No adverse effect was observed on ductility of the titanium alloy. Twin formation and the presence of very few dislocations in the processed material were the primary reasons for excellent tensile properties. Ahmed et al. [17] performed experimentation on cryogenic drilling of Ti–6Al–4V and compared its effectiveness with wet cooling in terms of cutting temperature and hole quality. According to their research, the cutting temperature reduces by maximum of 59% under cryogenic cooling. Bagherzadeh et al. [18] studied the effect of different cooling techniques on machinability of titanium turned samples. A mixture of minimum quantity CO_2 and oil (CMQL) was used and checked its effect on temperature and surface finish as compared to the other cooling techniques. CMQL increased tool life by 60% during turning of Ti–6Al–4V and machined surface finish was better as compared to CO_2 and MQL cooling methods. Microstructural study showed that the modified CMQL cooling technique reduced chip-tool contact length. Temperature study concluded that CMQL has higher heat extraction capacity as compared to other techniques. Dhananchezian [19] et al. studied the effect of liquid nitrogen on cutting temperature and surface topography using modified cutting tool insert in turning of Ti–6Al–4V. Cutting temperature was reduced by maximum of 66% and average surface roughness by maximum of 42% under the influence of cryogenic cooling over wet cooling approach during machining. Also, the supply of LN_2 through the holes made in the cutting tool insert was more effective as compared to the conventional methods. Hong et al. [20] evaluated cutting temperatures attained under different cooling techniques. Liquid nitrogen was directed through micro-jets to the rake and flank face on the cutting edge of the tool. A small amount of liquid nitrogen directed to the cutting edge was far better than the emulsion cutting in reducing the cutting temperature and finally resulted into better machined surface quality and integrity.

The above literature review shows that minimum quantity lubrication (MQL), flood cooling and cryogenic cooling have been used by researchers for improving tool life and integrity of machined surfaces. They studied the effect of cutting parameters and cooling techniques on microstructural changes and micro-hardness. They also studied the effect of liquid nitrogen on deformation of Ti–6Al–4V in terms of twin formation in grain structure, and the effect of

microstructural modifications on machinability of titanium alloys using laser heat treatment. Further, very few research works have been reported changes in microstructure on and below the drilled surfaces under various cryogenic temperatures. Therefore, in this study, a heat-sink-based cryogenic cooling was used in drilling of Ti–6Al–4V to understand its effect on the integrity of machined surfaces in terms of evaluated microstructural alterations and nano-hardness. This paper is organized as follows.

Experimental Work

Theme of Work

In this work, systematic experiments were performed to investigate the effect of heat-sink-based cryogenic cooling on surface integrity, and the theme of experimentation is shown in Fig. 1. Drilling experiments were performed on solutionized samples under dry and cryogenic cooling environments. Three different cryogenic cooling temperatures were selected to investigate its effectiveness on surface integrity of drilled surfaces. For the mechanical characterization of drilled surfaces and sub-surfaces and the evaluation of the microstructure of drilled holes, the holes were sliced along their axes. The microstructural changes were image quality, twin formation, machining affected zones, the grain boundaries with low and high angles, kernel average misorientation (KAM) and nano-indentation hardness. More details of the experimental procedure are described in the following sections.

Work and Tool Materials

Commercially available titanium (Ti–6Al–4V) alloy was procured to investigate the surface integrity after drilling. Table 1 displays the chemical constitution of titanium alloy. Titanium alloy (Ti–6Al–4V) samples were solutionized in vacuum muffled furnace at 900 °C for 4 hours. Each drilling experiments was performed using a new uncoated a carbide drill with a 6.35-mm diameter on solutionized sample having dimensions 150 × 20 × 7 mm.

Experimental Set-up

Drilling tests were conducted using Hardinge VMC-600 II. Titanium workpiece was attached on the heat-sink channel made of highly conductive copper plate and mounted on a KISTLER piezoelectric dynamometer. Dynamometer cables were coupled to a charge amplifier and a data acquisition system for recording drilling-related thrust and torque data. Temperature measurements were taken in the cutting zone using an infrared thermal camera (FLIR brand). Cryogenic tank was used to store liquid nitrogen and was equipped with inlet and outlet hose pipe connections. A liquid nitrogen gas cylinder was connected with cryogenic tank through the pipe connection and a regulator.

Experimental Procedure

A total of 12 drilling experiments were performed and were repeated twice to ensure repeatability. Three different cryogenic temperatures were maintained during drilling; they are

Fig. 1. Theme of experimentation

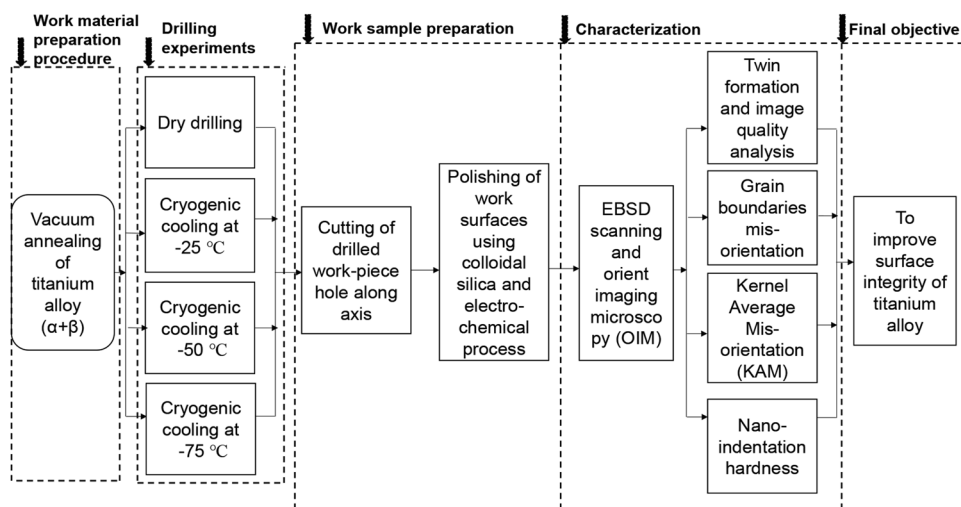


Table 1. Chemical elements of titanium alloy

Element	Ti	Al	V	Fe	N	O	H	C
wt. %	90	6.1	3.8	0.36	0.029	0.13	0.00198	0.029

as $-25\text{ }^{\circ}\text{C}$, $-50\text{ }^{\circ}\text{C}$ and $-75\text{ }^{\circ}\text{C}$. Pressure of the nitrogen gas was maintained at 1 bar throughout the experimentation. RTD (resistance temperature detector) sensors were attached at the top face of workpiece at two different locations and were connected to a microcontroller to maintain cryogenic temperatures. In the entire drilling process, two different cutting speeds of 65 and 95 m/min and two feeds of 0.1 and 0.2 mm/rev were used.

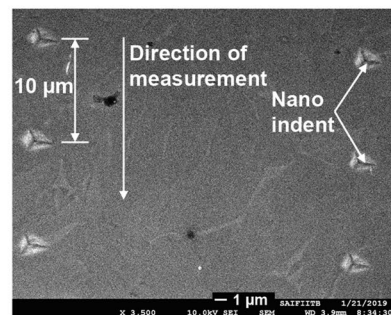
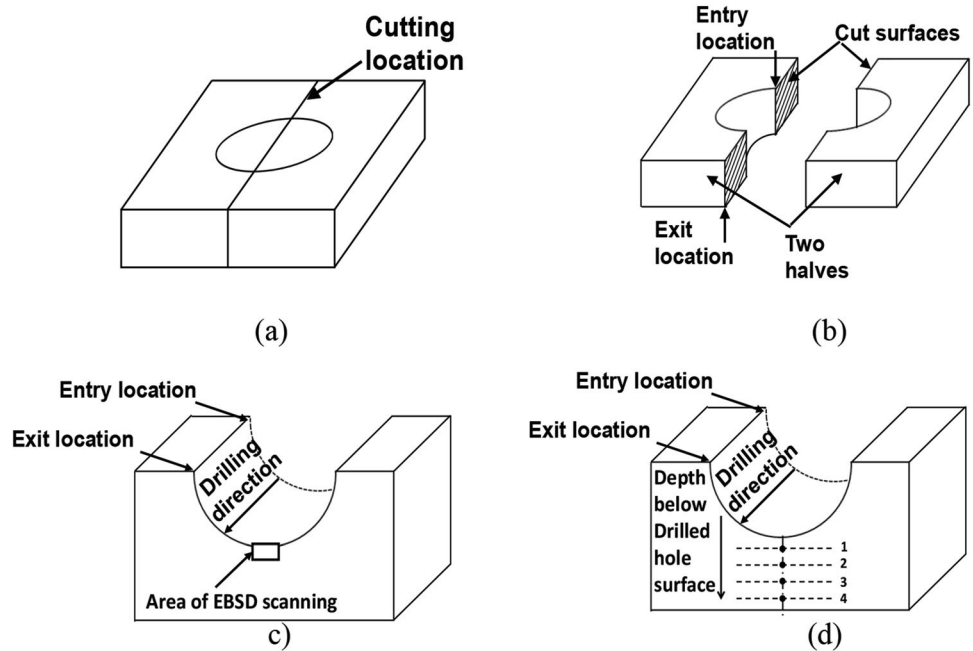
Microstructure Analysis and Nano-Hardness measurement

Drilled holes were cut into two splits using wire EDM machine (Fig. 2a–b). The split samples were cleaned with ultrasonic cleaning bath and were polished using prescribed polishing procedure on an automatic polishing machine.

Colloidal silica of $0.5\text{ }\mu\text{m}$ (OP-S) mixed with half water was used for mirror polishing. Electro-polishing was used to achieve improved surface quality using electrolyte solution by mixing perchloric acid 80 % and methanol 20%. Oxford EBSD detector mounted on GEMINI SEM 300 was used with 20 KeV accelerating voltage and $0.3\text{ }\mu\text{m}$ step size to gather crystallographic data near exit surfaces of the drilled hole samples (Fig. 2c). TSL orient imaging microscopy software was used to quantify EBSD data such as inverse pole figure (IPF) map, misorientation analysis, image quality (IQ), low- and high-angle boundaries of grains and kernel average misorientation (KAM).

Hysitron TI-900, Bruker machine was used for nano-indentation. Nano-hardness was measured at every $10\text{ }\mu\text{m}$ distance along the drilled sub-surface at exit side of the drilled holes using a nano-indenter (Fig. 2d–e).

Fig. 2 a Cutting location of drilled hole b drilled hole cut into two halves c area of EBSD scanning at the drilled hole exit surface d drilled hole entry and exit location showing hardness measurement points 1-4 and e nano-indentation contour



(e)

Results and Discussions

As-received titanium plates were annealed at 900 °C for 4 hours in a vacuum furnace. Grain size of the as-received sample increased from 4.8 to 10 μm due to recrystallization. After annealing process, grains were found more equiaxed as compared to the as-received material (see Fig. 3). Similar results were stated by Telrandhe et al. [5]. Previous research has shown that the exit surfaces of drilled hole suffer from substantial distortion relative to the entering locations. [21]. As a result, a detailed investigation of exit surfaces of drilled halves has been performed.

Microstructural Evolution of the Machined Surfaces

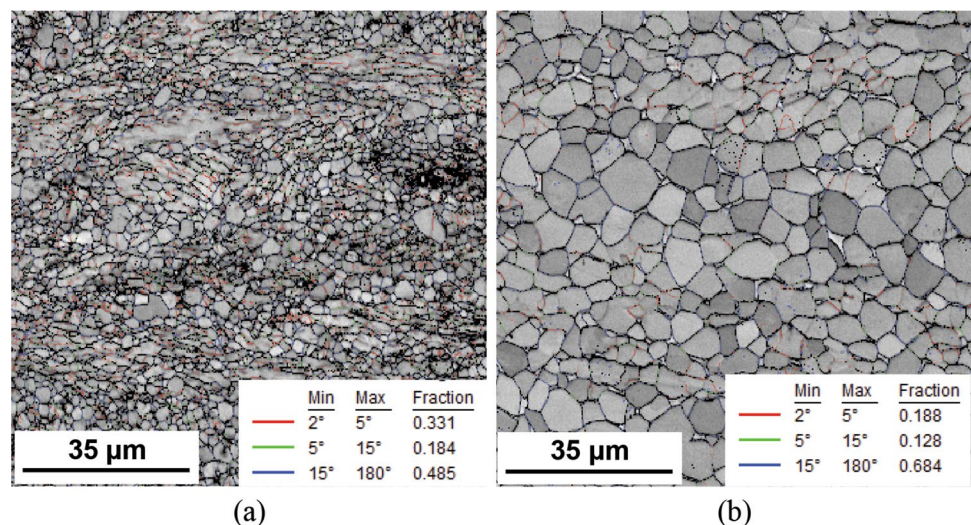
During drilling, sub-surfaces below the drilled hole experience mechanical and thermal stresses which cause microstructure alterations in this region [22]. To understand the microstructural changes, EBSD data at the exit surfaces of drilled hole were gathered. The IPF maps generated for various drilling conditions are shown in Figs. 4 and 5. Two different zones are observed near the drilled surfaces: one that has larger portion of points without indexing, and the other, with a comparatively lesser portion of points without indexing (black), as shown in Fig. 4a. The zone B in Fig. 4a, which has a lower percentage of points without indexing, represents a grain structure with lower deformation since it is in the region away from the machined surfaces, whereas the area with a higher proportion of points without indexing exhibits a severe grain deformation, as observed in zone A in Fig. 4a. In dry drilling, temperature is generated at tool-workpiece interface resulting in high sticking friction between them which causes the high sub-surface

deformation, whereas in cryogenic cooling, temperature at the interface was comparatively lower than in dry drilling.

A severely non-indexed zone is observed near the drilled edge during dry drilling at cutting speeds of 65 m/min and feed rates of 0.1 mm/rev, whereas an adequately indexed zone is observed in cryogenic cooling at -25 °C (Fig. 4b), -50 °C (Fig. 4c) and at -75 °C (Fig. 4d). Moreover, grains in the sub-surface region elongate along the cutting direction in dry drilling (Fig. 4a), although this was not the case during cryogenic chilling (Fig. 4b–d). Additionally, dry drilling at cutting speeds of 65–95 m/min results in an intensification of the non-indexing region (Fig. 4e) representing severity of plastic deformation near the drilled surfaces, whereas in the cryogenically cooled drilled samples, intensity of non-indexing zone is found comparatively lower than in dry drilling (Fig. 4f–h). With a change in feed rate from 0.1 to 0.2 mm/rev, temperature rise at the interface increases which results in the formation of a large non-indexed zone in dry drilling (Fig. 5a). Alternatively, the non-indexed zone was not observed for the cryogenic cooling at -25 °C and -50 °C and at cutting speed of 65 m/min, as shown in Fig. 5b–c. It was further observed that the hardness along with brittleness of the material increases with increasing cryogenic cooling temperature [23]. Therefore, for cryogenic temperature of -75 °C, micro-cracks with non-indexed locations were observed near the drilled surfaces. This could be due to comparatively higher brittleness in the samples (Fig. 5d).

Similarly, by increasing the feed from 0.1 to 0.2 mm/rev, a heavy non-indexed zone is evident in dry drilling (Fig. 5e). In the cryogenic cooled samples, a substantial amount of non-indexed zone is observed. This could be due to higher brittleness on the drilled surfaces (Fig. 5f–h). It is observed that the sub-surface deformation in the cryogenic cooled samples is lower than in the dry drilled ones, under

Fig. 3 Misorientation of low- and high-angle grain boundaries for **a** as-received and **b** annealed Ti-6Al-4V [21]. Reprinted from Materials Today Communications, Vol. 26, Dipesh B. Trivedi, Jitesh Vasavada, Suhas S. Joshi, Microstructural assessment of drilled cross sections on titanium generated under different cooling strategies, pg. 101954, Copyright 2021, with permission from Elsevier



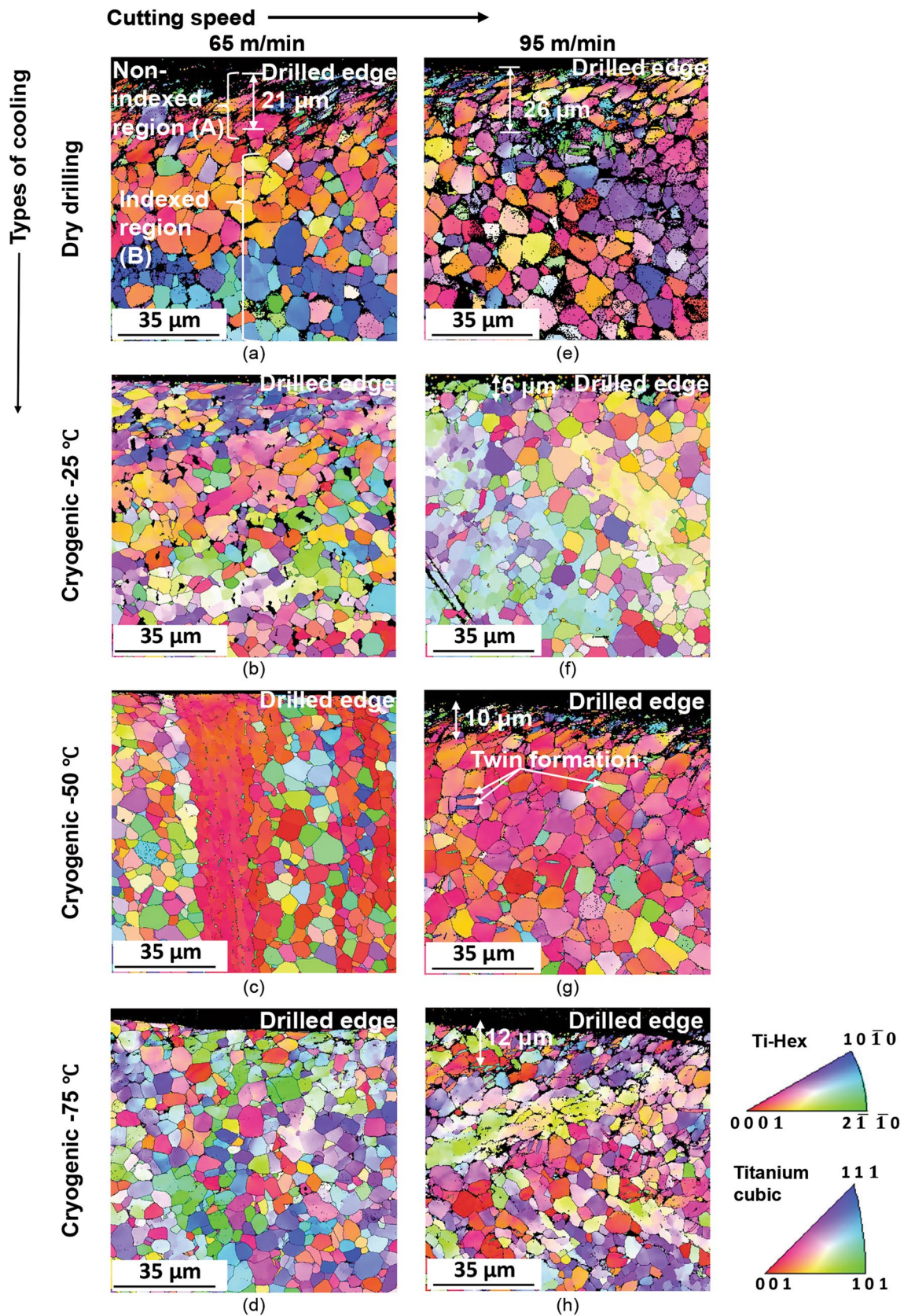
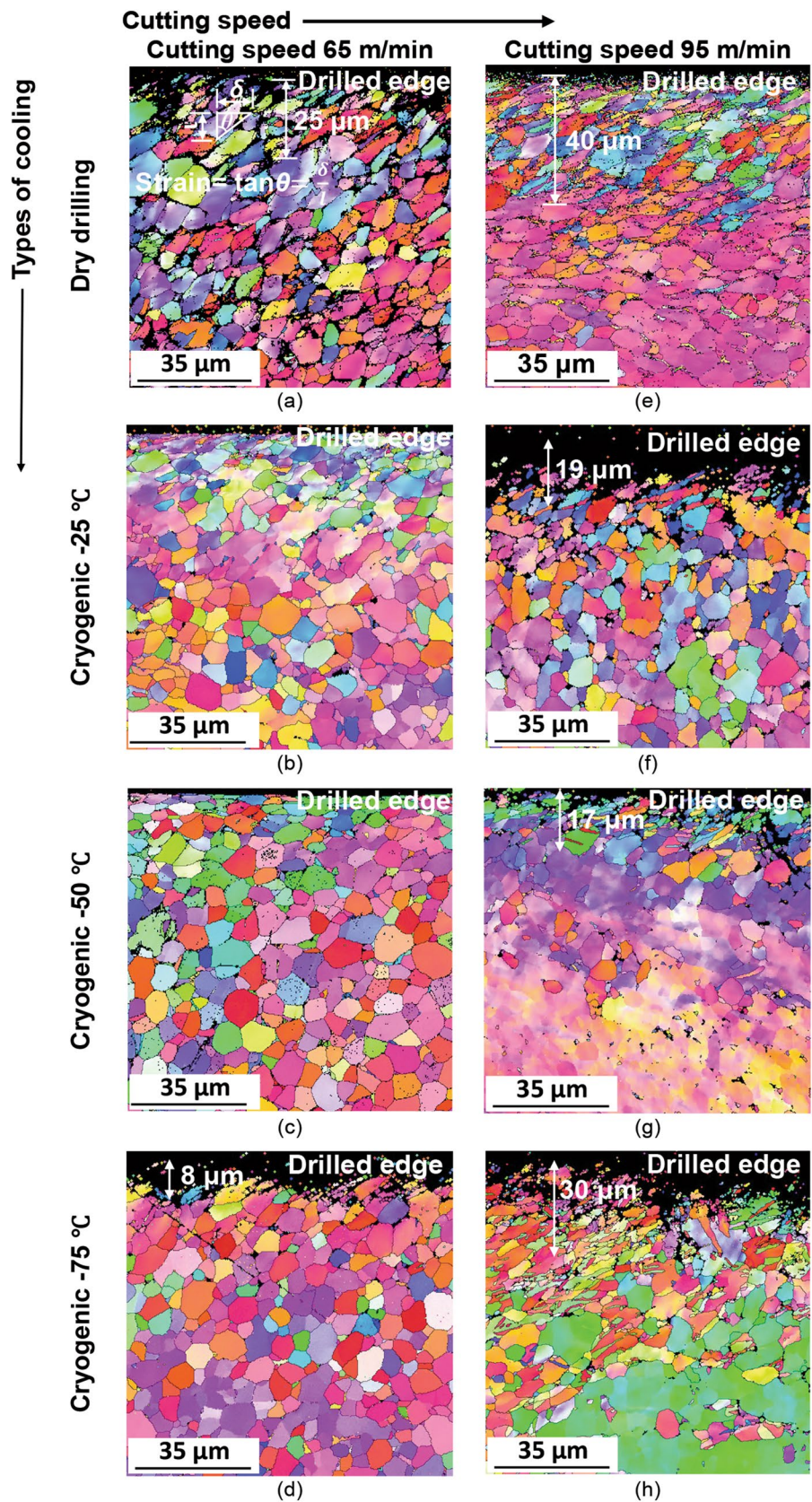


Fig. 4 a–h Inverse pole figure (IPF) maps with grain morphology and orientation for exit location of drilled hole surfaces on Ti–6Al–4V samples at 0.1 mm/rev feed rate and under different cooling conditions

Fig. 5 a–h Inverse pole figure (IPF) maps with grain morphology and orientation for exit location of drilled hole surfaces on Ti–6Al–4V samples at 0.2 mm/rev feed rate and under different cooling conditions



all cutting conditions. This would be because of reduced thermal load and the corresponding lower cutting zone temperatures.

Machining Affected Zone (MAZ)

During drilling, grains get deformed and elongate in cutting direction below the drilled surfaces and the region over which the deformation occurs is called machining affected zone (MAZ). The depth of the machining affected zones (MAZ) for the different cutting and cooling conditions is shown in Figs. 4a–h and 5a–h. The average MAZ in dry drilling is quantified as 21 μm at 65 m/min cutting speed and 0.1 mm/rev feed rate (Fig. 4a). For the same feed and speed, negligible MAZ is observed in cryogenic cooling conditions at $-25\text{ }^\circ\text{C}$, $-50\text{ }^\circ\text{C}$ and $-75\text{ }^\circ\text{C}$, as shown in Fig. 4b–d. Cryogenic cooling has a potential to reduce friction at the tool-workpiece interface that finally results into a reduction in the cutting temperature. It causes a reduction in plastic strain near the drilled surfaces and the strain reduces further along the depth of deformation beneath the drilled surface. Therefore, at 65 m/min cutting speed 0.1 mm/rev feed, cryogenically cooled samples do not show any MAZ. Further, in dry drilling, the average machining affected zone increased by 26 μm as cutting speed increased from 65 to 95 m/min (Fig. 4e). However, under the same cutting conditions, the average MAZ was found to be 6 μm , 10 μm and 12 μm in the cryogenically cooled samples at $-25\text{ }^\circ\text{C}$, $-50\text{ }^\circ\text{C}$ and $-75\text{ }^\circ\text{C}$, respectively, as shown in Fig. 4f–h.

However, increasing the feed from 0.1 to 0.2 mm/rev, MAZ increases from 21 to 25 μm (Fig. 5a) due to high heat generation and plastic deformation during dry drilling process. With increasing feed rate to 0.2 mm/rev, the cryogenically cooled samples at $-25\text{ }^\circ\text{C}$ (Fig. 4b) and $-50\text{ }^\circ\text{C}$ (Fig. 4c) show a lower MAZ in a comparison with the corresponding dry drilled samples (Fig. 4a), whereas a significant increase in MAZ by (8 μm) is observed in the cryogenically drilled samples at $-75\text{ }^\circ\text{C}$ (Fig. 4d).

Moreover, as cutting speed and feed are increased, temperature rises, causing workpieces to become thermally softened and stick to the drill's cutting edge. Further increase in the feed rate requires more power to remove the increased volume of work material; consequently, it increases the drilling forces. Therefore, at the higher cutting speed, the average MAZ measured was 40 μm in dry drilling with feed of 0.2 mm/rev which is the highest value under all cutting conditions and cooling techniques tested here (Fig. 5e). Basavarajappa [24] et al. also reported similar deformation of sub-surfaces with increasing feed rate. Further, at the higher cutting speed, the average MAZ increases to 19 μm , 17 μm and 30 μm on the cryogenically cooled samples while drilling at $-25\text{ }^\circ\text{C}$, $-50\text{ }^\circ\text{C}$ and $-75\text{ }^\circ\text{C}$, respectively, as shown in Fig. 5f–h.

Analysis of Strain in Grains

As discussed earlier, the microstructure of titanium work material below the machined surfaces undergoes a significant change. As a result, considerable strains are introduced in the grains in this area along the drilling direction. The depth of machining affected zone (MAZ) was measured from the IPF maps of the titanium machined surfaces under different cutting and cooling conditions. Further, the grain elongation was also evaluated as strain in terms of the angle θ measured using ImageJ software, as shown in Fig. 6. Knowing θ , the strain in the grains was calculated using the following equation:

$$\varepsilon = \tan \theta = \frac{\delta_g}{l_g} \quad (1)$$

where δ_g is the grain deformation component along the machined surface, whereas l_g is the grain deformation component across the machined surface.

Figure 7a and b illustrates the variation in strain in the machining affected zone under dry and cryogenic cooling conditions at the feed rate of 0.1 and 0.2 mm/rev, respectively. As shown in Fig. 7a, at the 5 μm distance from the drilled edge, very high strain is observed among all the cutting and cooling conditions, whereas the strain reduces as we move from machined surface to sub-surface region. A high value of strain of 3.2 is seen in dry drilling at the cutting speed of 95 m/min and the feed rate of 0.1 mm/rev which is higher than other cryogenic cooling conditions, as shown in Fig. 7a. On the other hand, as shown in Fig. 7b, as feed rate increases from 0.1 to 0.2 mm/rev, and similar high strain is observed at 5 μm distance from the drilled edge under all cutting and cooling conditions. The maximum

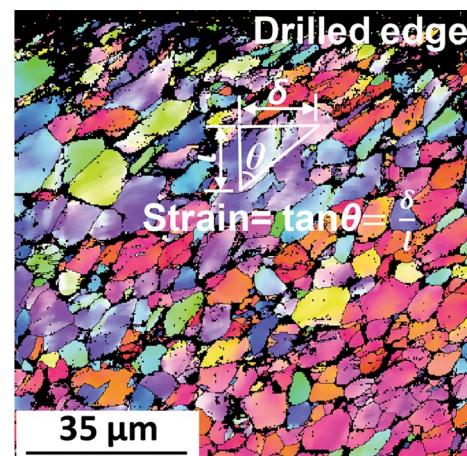
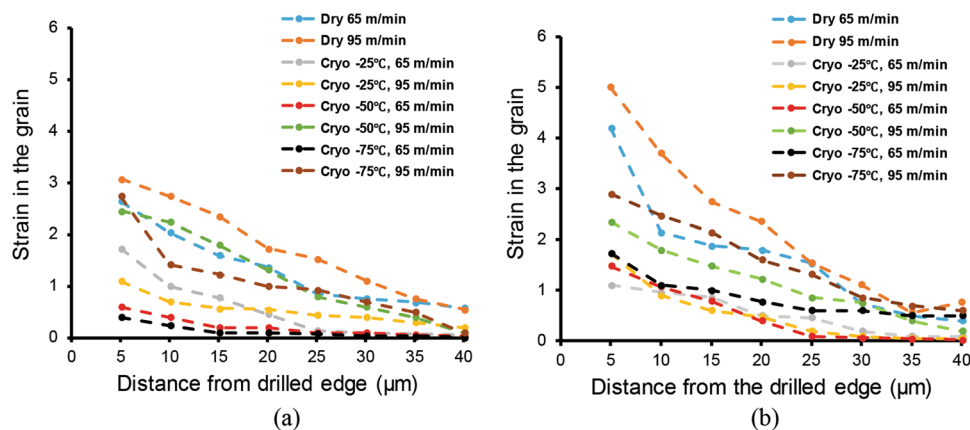


Fig. 6: IPF image showing components of strain measurement in a grain of titanium machined surface and sub-surface at the cutting speed of 65 m/min and feed rate of 0.2 mm/rev

Fig. 7 Variation in strain Vs distance from the drilled edge at different cutting speeds and under dry and different cryogenic cooling keeping feed rate at **a** 0.1 mm/rev and **b** 0.2 mm/rev



strain measured is 5 at the cutting speed of 95 m/min which is 63% higher as shown in Fig. 7b. It was evident that at the low cutting speed, the amount of heat generation is low and increases cutting speed. It is further evident from the graphical representation in Fig. 7a–b that the high feed rate results into higher value of strain in the grains. As compared to dry drilling, the cryogenic cooling makes the work material brittle. This is one of the reasons that a lower strain is observed in the work material before fracture under all cryogenic cooling conditions [4].

Annealing and Deformation Twinning

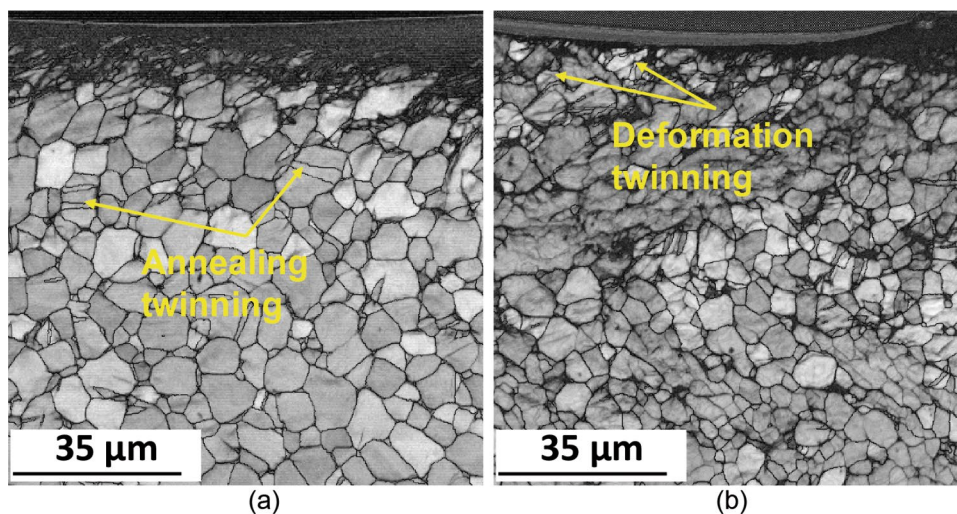
Twinning is a mechanism of plastic deformation. It arises when the work material is under the influence of thermal loading or deformation. Thermal loading results into annealing twins, whereas mechanical loading produces deformation twins. It is also understood that at the higher annealing temperature, due to larger grain size, the twin formation increases. In on work during cryogenic cooling, the deformation twins are observed near the drilled surface, where

grains are elongated or deformed along the drilling direction. The twins are also found below the machined surfaces or sub-surfaces, at higher levels of cutting speeds and cryogenic temperatures as shown in Fig. 8a–b. It is also evident that in the deformed regions, deformation twins are observed on the annealed and drilled samples of titanium due to a larger grain size. Double twinning is also observed inside a grain which is due to high strain rate with high deformation [5]. Low cryogenic temperature increases density of dislocations which increases the plasticity and also the twin formation in the microstructure [8].

Image Quality Analysis (IQ)

As mentioned earlier, a region near the drilled surface undergoes deformation during drilling which can be characterized using image quality index (IQ) [25, 26]. To compare IQ values of microstructures of different drilled samples, normalized IQ value ($IQ_{\text{Normalized}}$) was calculated from absolute IQ values obtained from EBSD data experiments based on equation [27],

Fig. 8 Twin formation in Ti–6Al–4V drilled samples at the cutting speed of 95 m/min and feed rate of 0.1 mm/rev under cryogenic cooling at **a** –50 °C and **b** –75 °C



$$IQ_{\text{Normalized}} = \frac{IQ_{\text{Absolute}} - IQ_{\text{Min}}}{IQ_{\text{Max}} - IQ_{\text{Min}}} \times 255 \quad (2)$$

where IQ_{Absolute} is the absolute value of image quality calculated from each scan, IQ_{Max} is the highest value of image quality, and IQ_{Min} is the lowest value of image quality. A magnified view of image quality (IQ) map is shown in Fig. 9 to get a normalized IQ value using equation (1). As presented in Fig. 9, starting from the top edge at the exit side of a drilled hole surface, the image quality (IQ) map is taken at each 10 μm distance in the sub-surface area. A region with higher $IQ_{\text{Normalized}}$ value indicates less strain

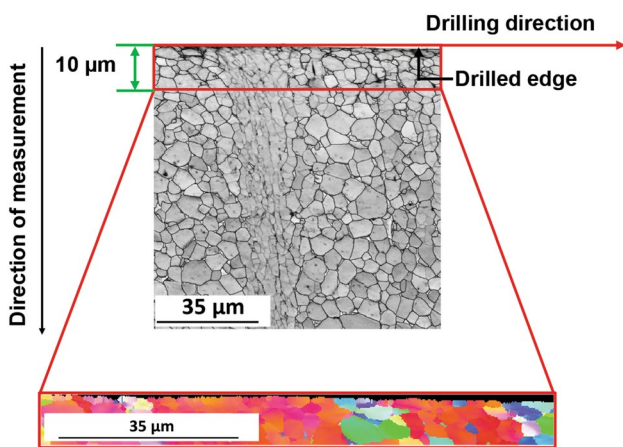


Fig. 9 Magnified view of the IQ map for achieving of normal IQ number in cryogenic cooling (-50 °C) at 65 m/min cutting speed and 0.1 mm/rev feed rate

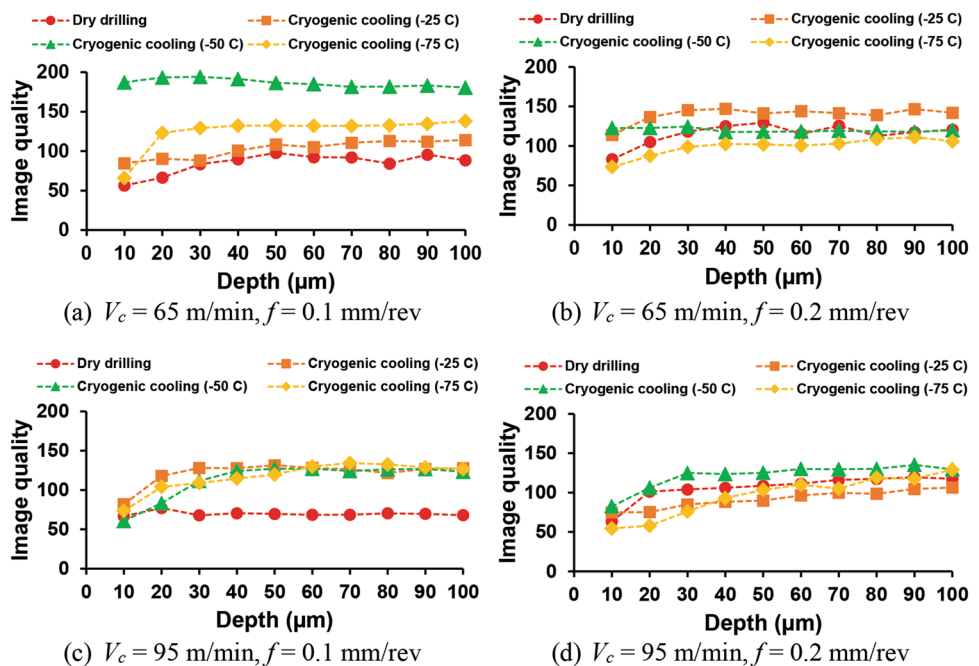
as compared to the region having lower $IQ_{\text{Normalized}}$ value. Image quality difference along the depth of exit drilled hole surfaces under dry and cryogenic cooling conditions is plotted in Fig. 10a–d.

At the cutting speed of 65 m/min and feed of 0.1 mm/rev, normalized IQ values for dry drilling and cryogenic cooling at $-25\text{ }^\circ\text{C}$, $-50\text{ }^\circ\text{C}$ and $-75\text{ }^\circ\text{C}$ are obtained as 56, 85, 187 and 66, respectively, at 10 μm distance from the drilled edge (Fig. 10a). It is observed that the normalized IQ values under cryogenic cooling conditions are higher than the dry drilling condition which indicates less deformation.

Keeping cutting speed constant and changing feed from 0.1 to 0.2 mm/rev, the $IQ_{\text{Normalized}}$ is 123 for cryogenic cooling at $-50\text{ }^\circ\text{C}$ which is higher than $IQ_{\text{Normalized}}$ of dry drilling of 83; at $-25\text{ }^\circ\text{C}$, it is 114, and at $-75\text{ }^\circ\text{C}$, it is 73 as shown in Fig. 10b. For a low cutting speed, the value of $IQ_{\text{Normalized}}$ is very low for dry drilling which due to heavy localized plastic deformation (Fig. 10a). In the other hand, low value of $IQ_{\text{Normalized}}$ at $-75\text{ }^\circ\text{C}$ sample might due to brittle fracture in sub-surface region (Fig. 10b). Moreover, as distance progresses away from the drilled surface, the drilling induced deformation reduces which can be seen by the slight increase in the normalized IQ value as shown in Fig. 10a, b.

Further, with a feed rate of 0.1 mm/rev and a cutting speed increase from 65 to 95 m/min, the $IQ_{\text{Normalized}}$ values are 67 for dry drilling, 82 for cryogenic $-25\text{ }^\circ\text{C}$, 61 for cryogenic at $-50\text{ }^\circ\text{C}$ and 74 for cryogenic at $-75\text{ }^\circ\text{C}$ at 10 μm distance from the drilled surface (edge) as shown in Fig. 10c. At this point, 22%, 34% and 11% improvements over dry drilling are evident at $-25\text{ }^\circ\text{C}$ $-50\text{ }^\circ\text{C}$ and $-75\text{ }^\circ\text{C}$. Now as the feed increases to 0.2 mm/rev, for the cutting speed as

Fig. 10 a–d Variation in image quality (IQ) along the depth of the exit surfaces of drilled holes under dry and different cryogenic chilling circumstances



95 m/min, the calculated $IQ_{\text{Normalized}}$ values for dry drilling and cryogenic cooling at $-25\text{ }^{\circ}\text{C}$, $-50\text{ }^{\circ}\text{C}$ and $-75\text{ }^{\circ}\text{C}$ are 64, 75, 83 and 55, respectively, at $10\text{ }\mu\text{m}$ from the drilled surface (edge) as shown in Fig. 10d.

Cryogenic cooling at $-50\text{ }^{\circ}\text{C}$ shows improvement of 30%, 10% and 50% as compared to dry, cryogenic $-25\text{ }^{\circ}\text{C}$ and $-75\text{ }^{\circ}\text{C}$, respectively. As observed before for the low cutting speed and high feed rate, it can be noticed that $IQ_{\text{Normalized}}$ values of dry and cryogenic $-75\text{ }^{\circ}\text{C}$ are lower than cryogenic cooling at other temperatures as shown in Fig. 10d. Overall, it is clear that the cryogenic cooling using heat-sink at $-25\text{ }^{\circ}\text{C}$ and $-50\text{ }^{\circ}\text{C}$ gives minimum sub-surface deformation under most of the operating conditions considered here.

Analysis of Misorientation in Low- and High-Angle Grain Boundaries

To understand the grain boundary evolution in the sub-surface region of exit surface of a drilled hole on titanium alloy, different grain boundaries fraction areas were measured and highlighted in image quality map as shown in Figs. 11a–d and 12a–d. Normally, the grain boundaries having misorientation angle greater than 15° are considered as high-angle boundaries. If the misorientation between two adjacent grains is less than 15° , then the grain boundaries are considered as low-angle grain boundaries [28]. In both the above-mentioned figures, low-angle boundaries (2° – 5°) and high-angle boundaries (15° – 180°) are highlighted in red and blue color line, correspondingly. The grain boundaries with low angle made of dislocations group get accumulated due mechanical or thermal processing [29].

During drilling, sub-surface experience mechanical deformation result in the formation of sub-grain boundaries. The extent of formation of sub-grain boundaries depends upon the drilling conditions and process parameters. The decrease in low-angle grain boundaries (in %) under different cryogenic cooling conditions as compared to dry drilling is presented in Table 2. At the slower cutting speed of 65 m/min and feed rate of 0.1 mm/rev, the fraction reduction in grain boundaries with low angle (2° – 5°) on the hole exit surfaces at $-25\text{ }^{\circ}\text{C}$, $-50\text{ }^{\circ}\text{C}$ and $-75\text{ }^{\circ}\text{C}$ is about 15%, 63% and 56% over dry drilling, respectively (Fig. 11a–d). Further, as the cutting speed increases from 65 m/min to 95 m/min, 52%, 39% and 28% drops are observed in cryogenic cooling at $-25\text{ }^{\circ}\text{C}$, $-50\text{ }^{\circ}\text{C}$ and $-75\text{ }^{\circ}\text{C}$, respectively, over dry drilling (Fig. 11 e-h).

When the feed is increased to 0.2 mm/rev, cryogenic cooling at $-25\text{ }^{\circ}\text{C}$, $-50\text{ }^{\circ}\text{C}$ and $-75\text{ }^{\circ}\text{C}$, low-angle grain boundaries (2° – 5°) are reduced by 32%, 71% and 62%, respectively, compared to dry drilling (Fig. 12a–d).

At the same cutting speed, the grain boundaries low angle in cryogenic cooling at $-25\text{ }^{\circ}\text{C}$, $-50\text{ }^{\circ}\text{C}$ and $-75\text{ }^{\circ}\text{C}$ are

reduced by 13%, 10% and 11%, respectively, as compared to the dry drilling with increasing feed from 0.1 to 0.2 mm/rev (Fig. 12e–h).

For a given microstructure, sum of fraction of all boundaries (2 – 5° , 5 – 15° and 15 – 180°) is 1; therefore, increasing the low-angle boundaries fraction may result in a decrease in high-angle boundaries fraction. For dry drilling, low-angle boundaries fraction increases from 0.613 to 0.744 with increasing feed rate from 0.1 to 0.2 mm/rev at the cutting speed of 65 m/min as mentioned in Figs. 11a and 12e, respectively, while for the same drilling condition, high-angle boundaries fraction decreases from 0.268 to 0.163 with increasing feed from 0.1 to 0.2 mm/rev. Similar relation between low-angle grain boundaries and high-angle grain boundaries was found in all the conditions. To sum up, the formation of sub-grain boundaries in dry drilling is comparatively less for given drilling parameters as compared to cryogenic cooling conditions. Moreover, minimum fraction of low-angle boundaries was found in cryogenic $-50\text{ }^{\circ}\text{C}$ and $-75\text{ }^{\circ}\text{C}$ at low cutting speed compared to all other conditions.

Kernel Average Misorientation (KAM)

Misorientation evolution in sub-surface region was analyzed by measuring kernel average misorientation (KAM) for all the dry drilling and heat-sink-based cryogenic cooling conditions. KAM maps for all the drilling conditions are shown in Figs. 13a–d and 14a–d. KAM indicates localized misorientation within the grain. With deformation, the orientation of the crystal changes led to a change in KAM value. The KAM value is typically observed less than 1° in undeformed grain structures. As discussed, the machined surface experiences severe deformation resulting in higher dislocation density in the distorted zone of microstructure than the other zones [30]. The zones, away from the drilled surface, highlighted with blue color indicate low dislocation density regions which have KAM value between 0° and 1° . The region with 1° – 5° of KAM shows medium to high value highlighted in green to red color. The red color indicates the highly deformed region. As discussed, the temperature rise at the interface in dry drilling is comparatively more than the cryogenic cooling condition. It led to higher plastic deformation and dislocation generation in dry drilling as compared to other conditions. Therefore, the maximum dislocations density zone reduces by 50%, 75% and 100% in cryogenic cooling at $-25\text{ }^{\circ}\text{C}$, $-50\text{ }^{\circ}\text{C}$ and $-75\text{ }^{\circ}\text{C}$, respectively, as compared to the dry drilling at 65 m/min cutting speed and 0.1 mm/rev feed (Figs. 13a–d and 15a).

Similarly, with increasing speed to 95 m/min and keeping feed rate at 0.1 mm/rev, the sub-surface deformation is comparatively high than lower cutting speed. It leads to decrease in the fraction of KAM (0° – 1°) value, while the increase in

Fig. 11 a–h Image quality maps stating low-angle and high-angle grain boundaries dispersal at exit location of drilled hole surfaces of Ti–6Al–4V samples at different cutting speeds and 0.1 mm/rev feed rate under dry and cryogenic cooling environments (Inset of each map represents the color coding) (Color figure online)

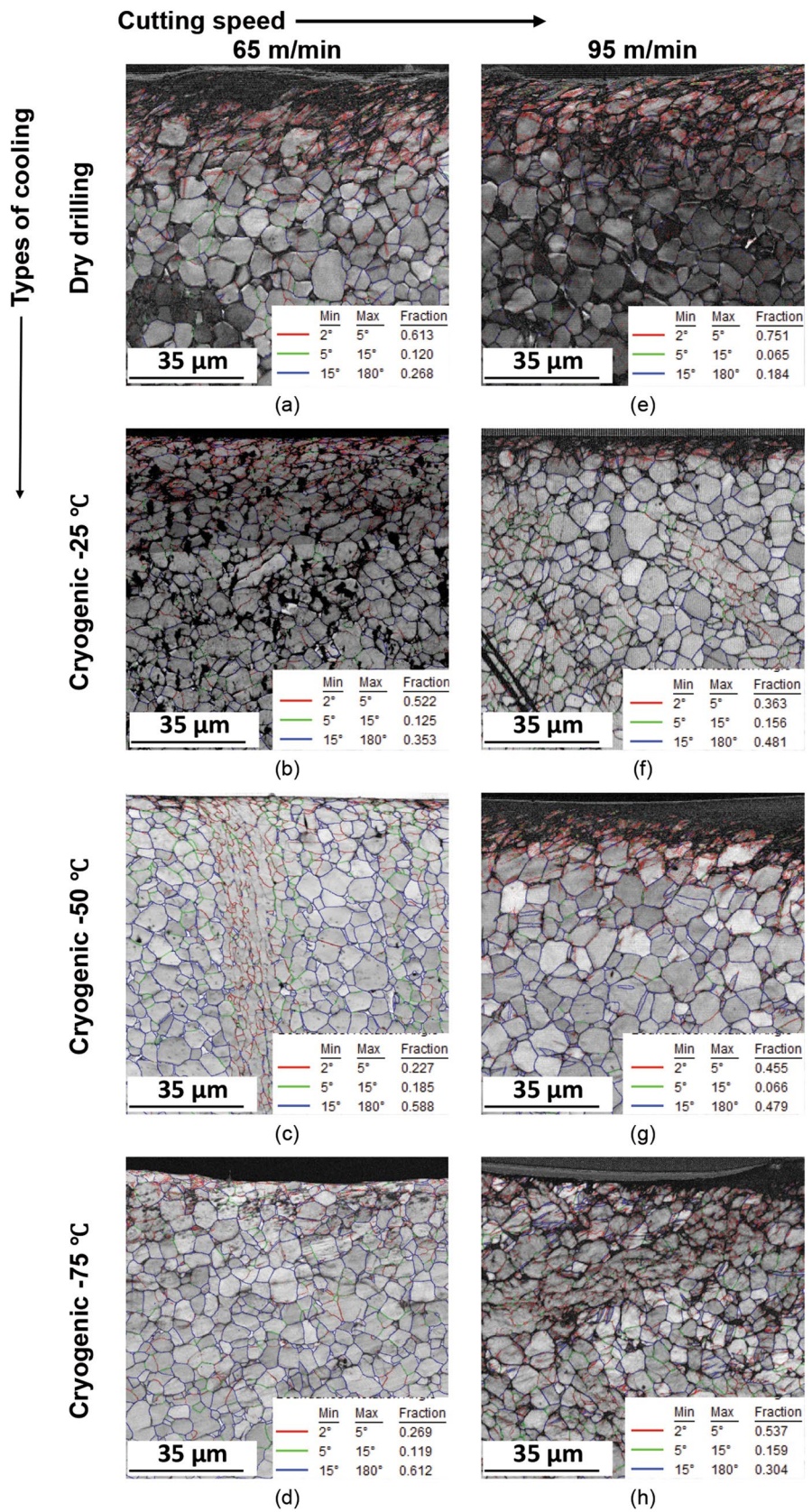


Fig. 12 a–h Image quality maps stating low-angle and high-angle grain boundaries dispersal at the exit location of drilled hole surfaces of Ti–6Al–4V samples at different cutting speeds and 0.2 mm/rev feed rate under dry and cryogenic cooling environments (Inset of each map represents the color coding) (Color figure online)

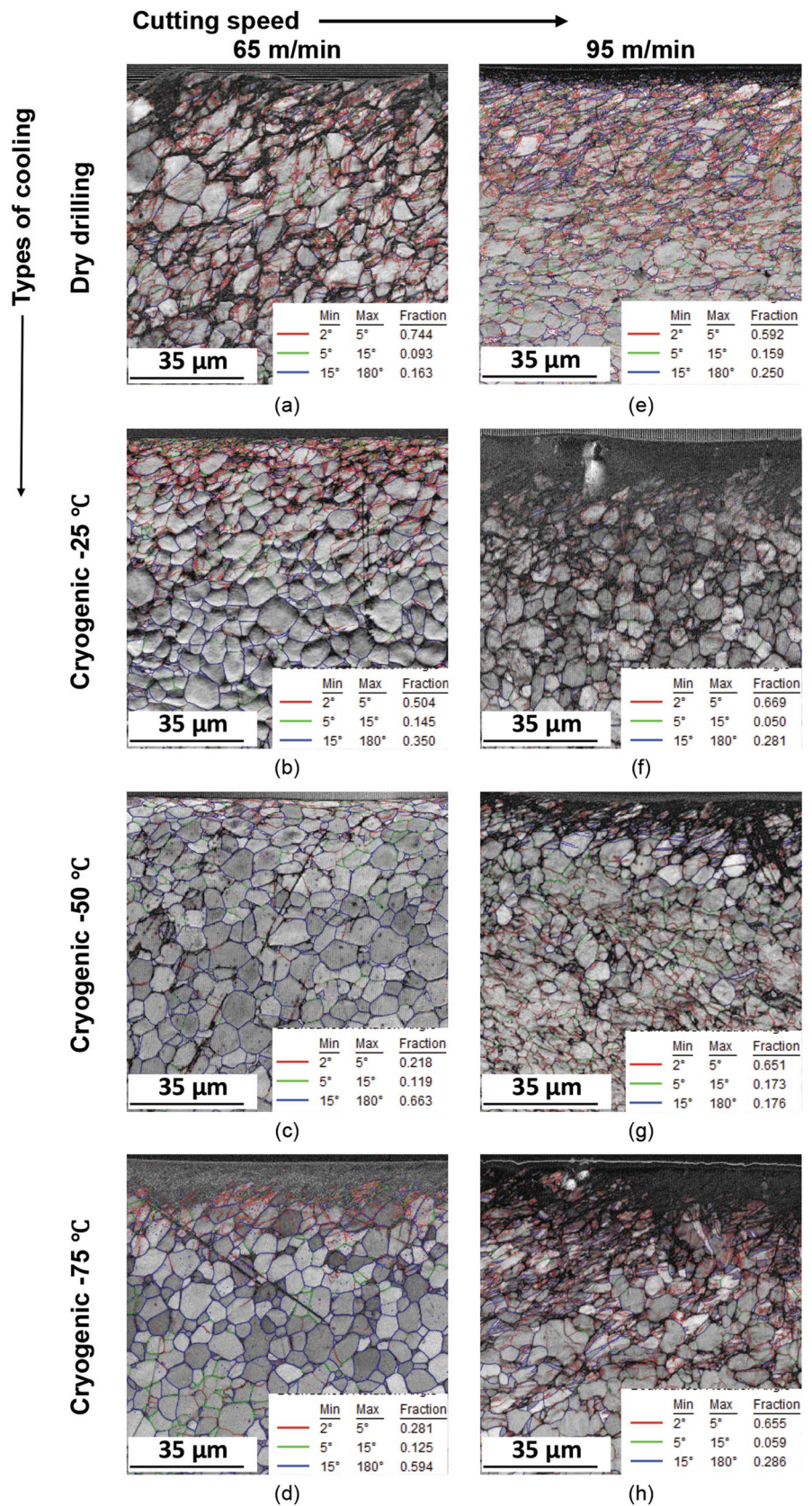


Table 2. Variation in grain boundaries with low angle (2° to 5°) at different cutting parameters and under dry drilling and different cryogenic temperatures

Cutting parameters	% decrease in low-angle grain boundaries (2° – 5°) with respect to dry drilling		
	At cryogenic -25°C	At cryogenic -50°C	At cryogenic -75°C
$V_c = 65$ m/min, $f = 0.1$ mm/rev	15	63	56
$V_c = 65$ m/min, $f = 0.2$ mm/rev	32	71	62
$V_c = 95$ m/min, $f = 0.1$ mm/rev	52	39	28
$V_c = 95$ m/min, $f = 0.2$ mm/rev	13	10	11

the fraction of KAM (1° – 3°) which shows the higher sub-surface deformation with increasing cutting speed for all the drilling conditions. The uppermost dislocation density area reduces by 33%, 33% and 50% in cryogenic -25°C , -50°C and -75°C cooling conditions, respectively, over dry drilling (Figs. 13e–h and 15c). At the cutting speed of 65 m/min, as the feed increases from 0.1 to 0.2 mm/rev, distribution of KAM shifts toward higher misorientation angle which indicates higher sub-surface deformation under all the drilling conditions as shown in Fig. 14a. Moreover, 40% and 20% reduction in misorientation was found in cryogenic -50°C and cryogenic -75°C cooling, respectively, over dry drilling (Figs. 14a–d and 15b).

At the speed 95 m/min, as the feed rate increases from 0.1 to 0.2 mm/rev, the average KAM values increase under all the cutting conditions, while 81%, 81% and 75% reduction in misorientation is observed in cryogenic cooling at -25°C , -50°C and -75°C , respectively, over dry drilling (Figs. 14e–h and 15d). It is observed that increasing the feed affects sub-surface deformation more as compared to the cutting speed. Kernel average misorientation shows a reduction in sub-surface deformation in the cryogenic cooling using heat-sink over dry drilling. Comparatively, cryogenic cooling at -25°C and -50°C at lower speed and feed rate appears to impart lower sub-surface deformation at cryogenic temperature of -75°C and in the dry drilling condition. At higher feed rate and cryogenic temperature -75°C , the local misorientation value is higher compared to cryogenic temperature of -25°C and -50°C ; this could be due to brittle fracture below the drilled surface as shown in Fig. 14f and h.

Mechanical Characterization of the Machined Surfaces Underneath the Impact of Dry and Cryogenic Cooling with Heat-Sink Approach

Nano-Hardness Measurements

Figure 16a–d illustrates graphical plots of nano-indentation hardness H (GPa) measured at different locations from the machined surface to sub-surface at various cutting speeds, feed rates and cryogenic cooling temperatures. At 65 m/min

cutting speed and 0.1 mm/rev feed rate, the nano-hardness in dry drilling is observed as the lowest, and it fluctuates as the drilled edge distance increases to sub-surface region at 20 μm distance from the drilling edge. The cryogenic cooled drilled hole surfaces show higher value of hardness as compared to dry drilling (Fig. 16a). During dry drilling, at 65 m/min cutting speed and 0.1 mm/rev feed rate, the highest nano-hardness of 5 GPa is observed near the drilled surfaces, whereas the maximum increment of 42% increment is observed in the hardness using cryogenic cooling at -25°C as compared to dry drilling. With increasing feed from 0.2 mm/rev, the nano-hardness increases by 28% (maximum) in cryogenic cooling at -25°C in comparison with dry drilling (Fig. 16b). On the other hand, as the cutting speed changes from 65 to 95 m/min keeping the feed constant as 0.1 mm/rev, the nano-hardness reduces to 4 GPa in dry drilling possibly due to thermal softening. In addition to this, maximum of 48% increment is found in hardness in the cryogenically cooled samples at -50°C as compared to the dry drilled samples. At the increased cutting speed, as feed rate varies from 0.1 to 0.2 mm/rev, very large hardness of 8 GPa is evident in the cryogenically cooled samples. This is double than the dry drilled samples hardness 4 GPa . Here, it is observed that as the feed rate increases, at the higher cutting speed of 95 m/min, a higher value of surface hardness is evident due to strain hardening as shown in Fig. 16c–d [14]. In general, 60% improvement is evident over the base nano-hardness in cryogenic cooling. The application of liquid nitrogen absorbs generated heat from the drilled surfaces. Therefore, the drilled surfaces cooled to a low temperature become harder as compared to dry drilled surfaces. Work hardening and microstructural changes due to machining play a very important role in increasing hardness of the machined surfaces [31]. Based on this investigation, it can be inferencing that cryogenic drilling with optimal temperature can improve sub-surface region as compared to dry drilling. Sub-surface region after drilling was quantified using different microstructural parameters such as IQ, KAM, and low- and high-angle boundary fraction. Further, nano-hardness was measured at the sub-surface for all the drilling condition to understand the effect of cryogenic temperature on material hardness. This research can be further extended to understand the chip morphology, surface roughness of the hole

Fig. 13 a–h Kernel average misorientation dispersal at the exit location of drilled hole surfaces of Ti–6Al–4V at different cutting speeds and 0.1 mm/rev feed rate under dry and cryogenic cooling environments (Inset of each map represents the color coding) (Color figure online)

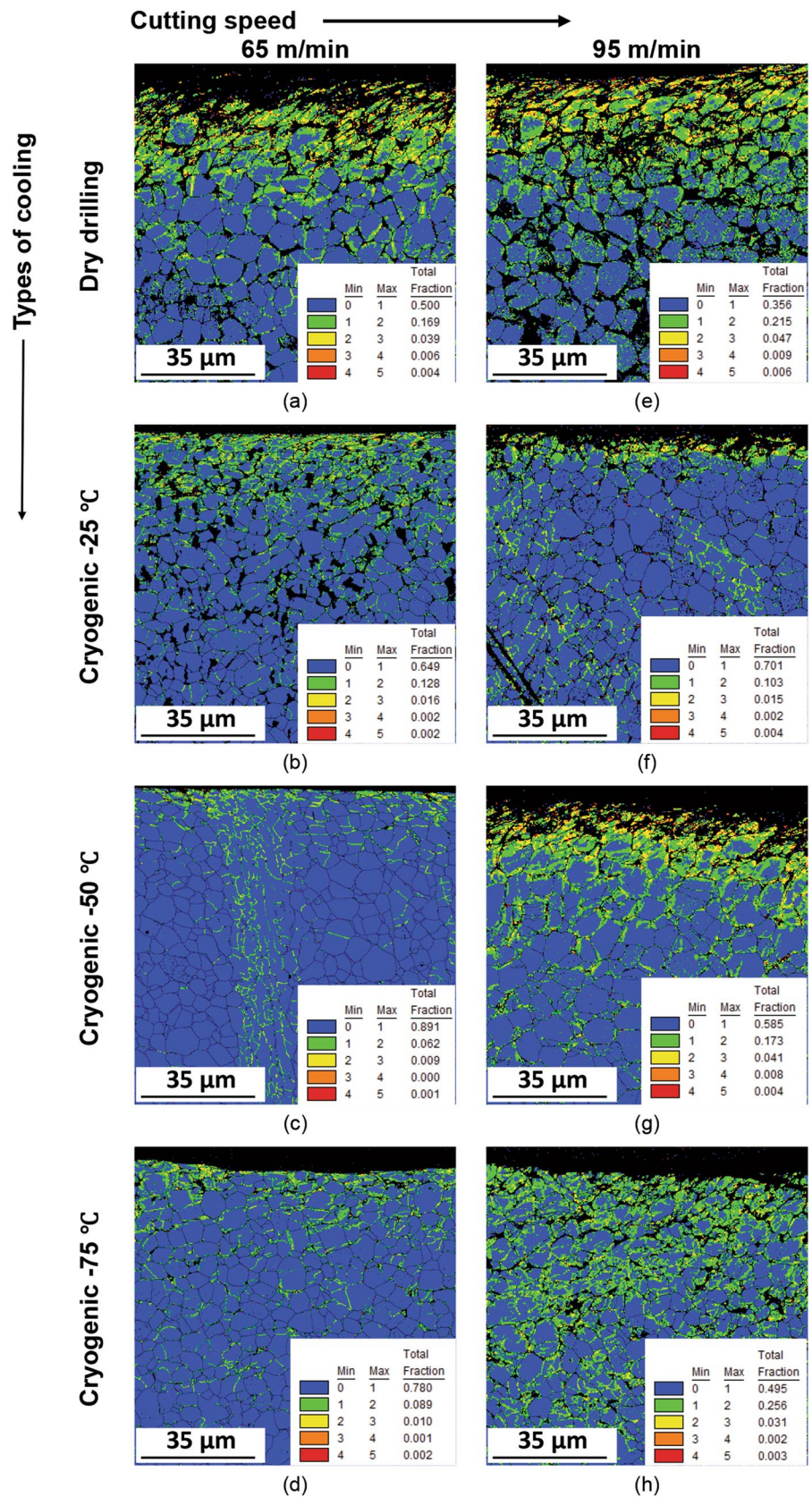


Fig. 14 a–h Kernel average misorientation distribution at the exit location of drilled hole surfaces of Ti–6Al–4V at different cutting speeds and 0.2 mm/rev feed rates under dry and cryogenic cooling environments (Inset of each map represents the color coding) (Color figure online)

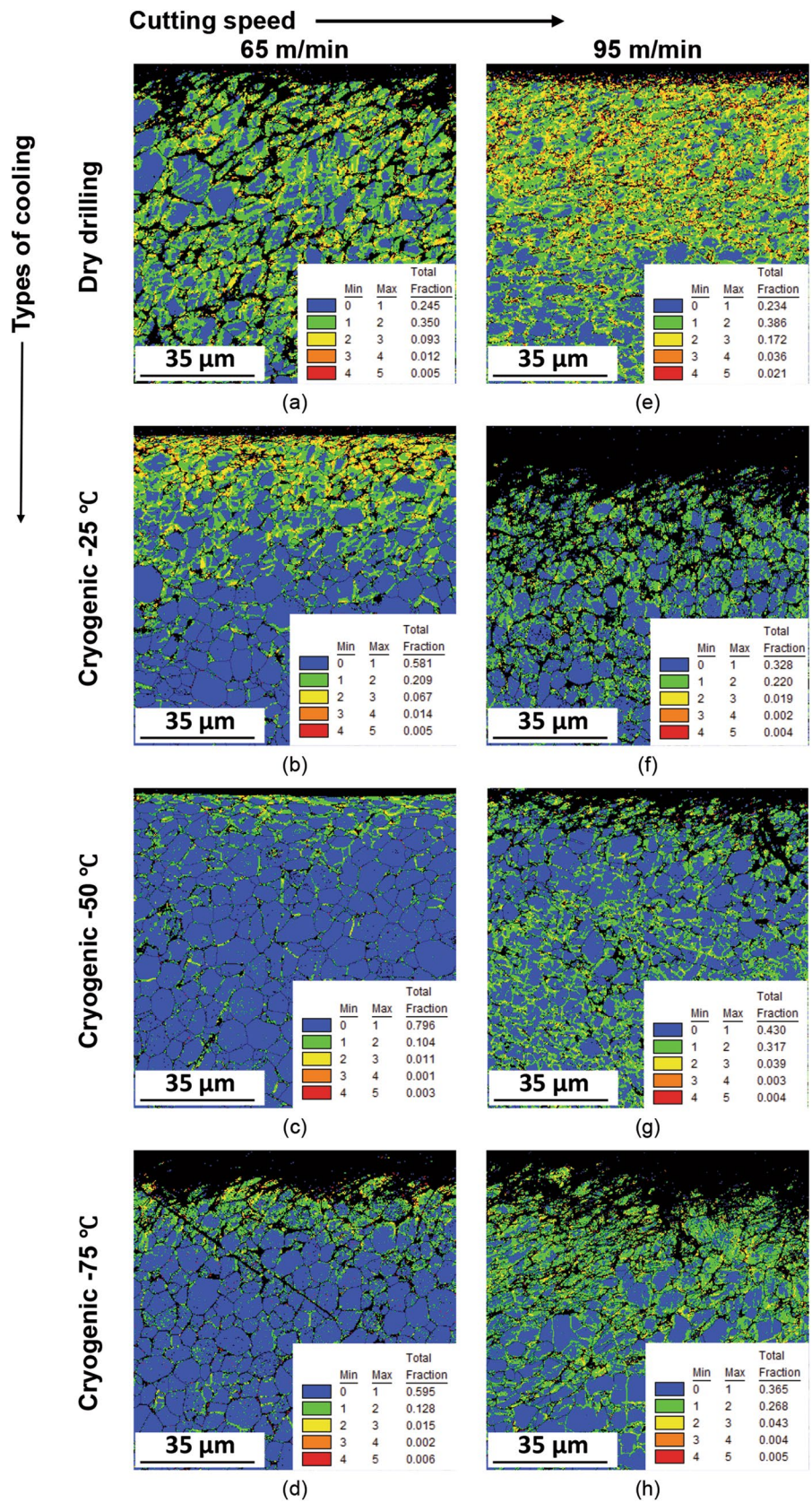


Fig. 15 a–d Graphical representation of low- to high-angle KAM values of titanium alloy drilled surfaces in dry and various cryogenic cooling conditions

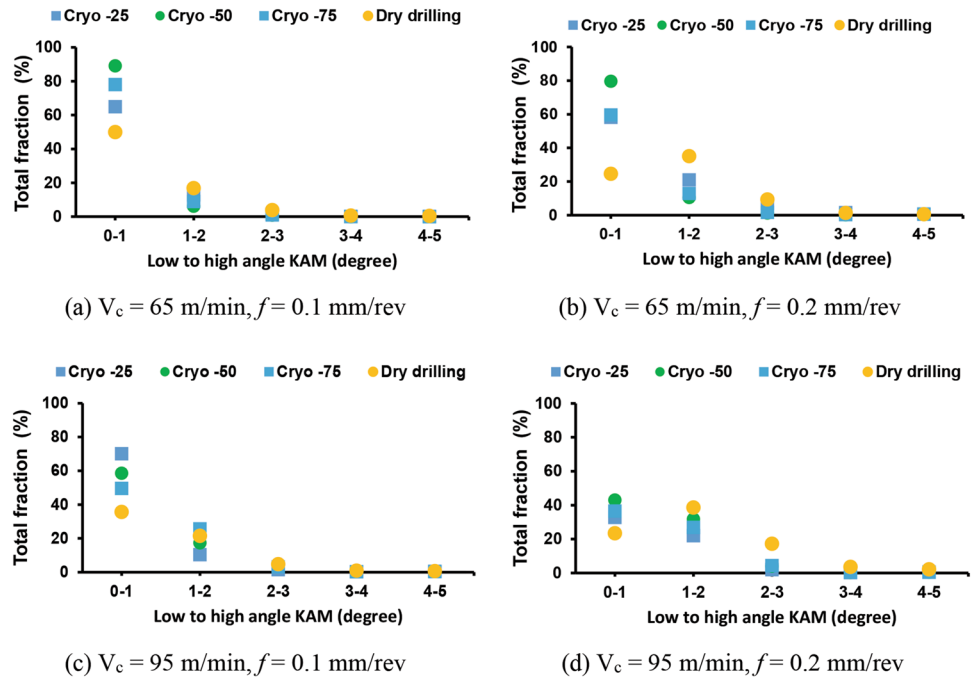


Fig. 16 a–d Nano-hardness profile of exit drilled hole surface under dry and cryogenic cooling conditions

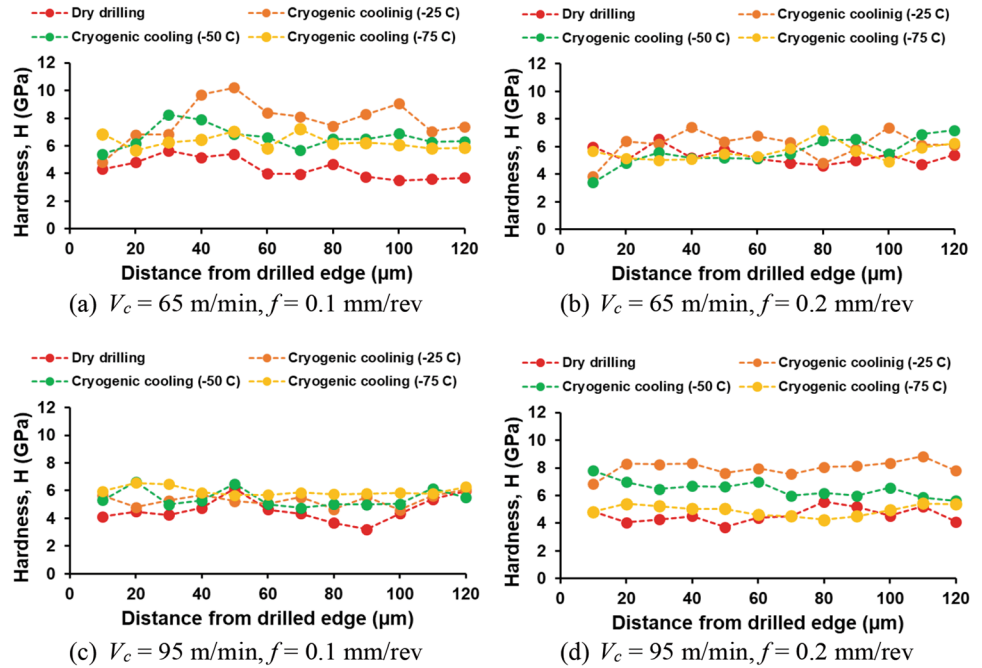


Fig. 17 Greatest and the poorest microstructural characterization parameters in dry and heat-sink-based cryogenic chilling methods depending on the cutting parameters

	DRY				NIR	CRYOGENIC				NIR	CRYOGENIC							
	DRY	CRYOGENIC -25 °C	CRYOGENIC -50 °C	CRYOGENIC -75 °C		DRY	CRYOGENIC -25 °C	CRYOGENIC -50 °C	CRYOGENIC -75 °C		DRY	CRYOGENIC -25 °C	CRYOGENIC -50 °C	CRYOGENIC -75 °C				
High Feed Rate 0.2 mm/rev	Heavy	Lowest	Lowest	Lowest	IQ	Heavy	Moderate	Moderate	Moderate	83	114	123	73	64	75	83	55	
	0.744	0.504	0.218	0.281	LAGB	0.592	0.669	0.651	0.655	0.163	0.35	0.663	0.594	0.25	0.281	0.176	0.286	
	0.005	0.005	0.003	0.006	KAM	0.021	0.004	0.004	0.005	25	Negligible	Negligible	8	40	19	17	30	
					MAZ													
Low Feed rate 0.1 mm/rev	Heavy	Lowest	Lowest	Lowest	IQ	Heavy	Lowest	Lowest	Lowest	56	85	187	66	67	82	61	74	
	0.613	0.522	0.227	0.269	LAGB	0.751	0.363	0.455	0.537	0.268	0.353	0.588	0.612	0.184	0.481	0.479	0.304	
	0.004	0.002	0.001	0	KAM	0.006	0.004	0.004	0.003	21	Negligible	Negligible	Negligible	26	6	10	12	
					MAZ													
Low Cutting Speed - 65 m/min						High cutting Speed - 95 m/min												
Key to Abbreviations: NIR- Non Indexed Region; IQ- Image Quality; LAGB - Low Angle Grain Boundaries; HAGB - High Angle Grain Boundaries; KAM - Kernel Average Misorientation; MAZ - Machining Affected Zone thickness (micrometer)																		
Best in red									Worst in blue									

and circularity of drilled hole after drilling under cryogenic cooling conditions.

Comparative Analysis of Characterization Parameters for EBSD

Figure 17 shows the finest and worst qualities of different parameters for EBSD characterization in terms of unindexed region (NR), impacted zone of machining (MAZ), image quality (IQ), misorientation in grain boundaries with low and high angle as well as kernel average misorientation (KAM) with reference to different cutting speed and feed rates.

From Fig. 17, it is detected that severity of the non-indexed zone is very high near the machined edge in dry drilling under all the cutting speeds and feed rates. On the other hand, the cryogenic chilling with heat-sink gives the least unindexed region; it denotes the uppermost region with no defect in the microstructure. Image quality (IQ) analysis revealed that the cryogenic cooling with heat-sink shows better results in terms of the higher value of standardized IQ value in comparison with dry drilling under all the cutting conditions. It is evident that a higher rate of IQ shows small depth of distorted grains, hence the presence of the highest defect-free microstructure. Grain boundaries with a low angle show higher misorientation in dry drilling at all cutting speeds and feeds, whereas the cryogenic cooling at low cutting speed and feed rate shows a significantly lower value. A better microstructure is observed in cryogenic cooling with heat-sink because of lower dislocations in comparison to dry drilling. Under all cutting conditions, heat-sink-based cryogenic cooling detects more high-angle grain boundaries than dry drilling. In the kernel average misorientation (KAM) analysis, the least value of KAM is noticed in the heat-sink-based cryogenic cooling, whereas a higher value of KAM is detected in dry drilling under all the cutting speeds and feed

rates. The drilled hole surface encounters severe shear loads and dislocations during dry drilling. The intensity of shear stresses and dislocations are very high near the drilled hole surface in dry drilling; therefore, the microstructure seems highly deformed, whereas the dislocation density is less in cryogenic cooling with heat-sink conditions.

Conclusions

EBSD analysis was performed. The cryogenic cooling with heat-sink gave the whole indexing of grain structure nearby the drilling edge. The reason behind this phenomenon is a lower tool-workpiece interface temperature as compared to dry drilling, which reduces sticking friction and sub-surface deformation. It also gave the least machining affected zone (MAZ) of 6 μm. Along with a reduction in cutting temperature, the cryogenic cooling reduced plastic strain near the drilled surfaces, and the strain reduced further along the depth of deformation below the drilled edge. This is one of the reasons of the least machining affected zone found in the cryogenic cooling.

The least value of strain in the grain of 0.4 was evident at the feed rate of 0.1 mm/rev and 1.1 at the feed rate of 0.2 mm/rev in cryogenic cooling with heat-sink. Also, as the strain increases, as the feed rate also increases proportionally. The cryogenic cooling makes work material brittle; hence, a lower strain is observed in the machined surfaces on titanium than in dry drilling.

Further, the heat-sink-based cryogenic cooling possesses the highest standardized image quality (IQ) value indicating the best microstructure (the maximum defect-free). The drilled hole sub-surfaces experience high strain and deformation in the grains. Therefore, they have lower value of image quality (IQ). On the other side, the cryogenic cooling with heat-sink indicated less strain and deformation, hence have a higher value of image quality (IQ).

In addition to above, it resulted into the least grain boundaries with a low angle. In dry drilling, dislocation density was high due to mechanical or thermal processing, whereas in cryogenic cooling with heat-sink, it was lower possibly due to low dislocation density.

The least value of kernel average misorientation (KAM) of 0.001 is observed in heat-sink-based cryogenic cooling. It was evident that in the undeformed grain structure, the value of KAM is less than 1° .

A comparatively higher value of nano-hardness of 8 GPa was observed in cryogenic chilling over dry drilling. The LN₂ absorbs the heat generated from the machined surfaces. Therefore, the machined surfaces that are cooled to a low temperature become harder. Work hardening and microstructural changes during machining increase hardness of machined surfaces.

Acknowledgements Authors would like to thank the Indian Government's Aeronautics and Research Development Board (ARD&B), for financial support and the Indian Institute of Technology Bombay for make available research facility.

References

- I.S. Jawahir, E. Brinksmeier, R. M'Saoubi, D.K. Aspinwall, J.C. Outeiro, D. Meyer, D. Umbrello, A.D. Jayal, Surface integrity in material removal processes: Recent advances. *CIRP Ann. Manuf. Technol.* **60**, 603–626 (2011). <https://doi.org/10.1016/j.cirp.2011.05.002>
- I.S. Jawahir, H. Attia, D. Biermann, J. Duflou, F. Klocke, D. Meyer, S.T. Newman, F. Pusavec, M. Putz, J. Rech, V. Schulze, D. Umbrello, Cryogenic manufacturing processes. *CIRP Ann. Manuf. Technol.* **65**, 713–736 (2016). <https://doi.org/10.1016/j.cirp.2016.06.007>
- S.Y. Hong, I. Markus, W.C. Jeong, New cooling approach and tool life improvement in cryogenic machining of titanium alloy Ti-6Al-4V. *Int. J. Mach. Tools Manuf.* **41**, 2245–2260 (2001). [https://doi.org/10.1016/S0890-6955\(01\)00041-4](https://doi.org/10.1016/S0890-6955(01)00041-4)
- S. Joshi, P. Pawar, A. Tewari, S.S. Joshi, Influence of β phase fraction on deformation of grains in and around shear bands in machining of titanium alloys. *Mater. Sci. Eng. A.* **618**, 71–85 (2014). <https://doi.org/10.1016/j.msea.2014.08.076>
- S.V. Telrandhe, A.K. Saxena, S. Mishra, Effect of microstructure and cutting speed on machining behavior of Ti6Al4V alloy. *J. Mech. Sci. Technol.* **31**, 2177–2184 (2017). <https://doi.org/10.1007/s12206-017-0413-9>
- S.V. Telrandhe, B. Jayabalan, C.P. Paul, S.K. Mishra, Microstructural development due to laser treatment and its effect on machinability of Ti6Al4V alloy. *Metall. Mater. Trans. A.* **49**, 3450–3467 (2018). <https://doi.org/10.1007/s11661-018-4728-7>
- Q. Wang, Z. Liu, Plastic deformation induced nano-scale twins in Ti-6Al-4V machined surface with high speed machining. *Mater. Sci. Eng. A.* **675**, 271–279 (2016). <https://doi.org/10.1016/j.msea.2016.08.076>
- K. Gu, H. Zhang, B. Zhao, J. Wang, Y. Zhou, Z. Li, Effect of cryogenic treatment and aging treatment on the tensile properties and microstructure of Ti-6Al-4V alloy. *Mater. Sci. Eng. A.* **584**, 170–176 (2013)
- S.W. Choi, J.W. Won, S. Lee, J.K. Hong, Y.S. Choi, Deformation twinning activity and twin structure development of pure titanium at cryogenic temperature. *Mater. Sci. Eng. A.* **738**, 75–80 (2018). <https://doi.org/10.1016/j.msea.2018.09.091>
- Z. Weng, K. Gu, C. Cui, H. Cai, X. Liu, J. Wang, Microstructure evolution and wear behavior of titanium alloy under cryogenic dry sliding wear condition. *Mater. Charact.* **165**, 110385 (2020). <https://doi.org/10.1016/j.matchar.2020.110385>
- M.J. Bermingham, J. Kirsch, S. Sun, S. Palanisamy, M.S. Dargusch, New observations on tool life, cutting forces and chip morphology in cryogenic machining Ti-6Al-4V. *Int. J. Mach. Tools Manuf.* **51**, 500–511 (2011). <https://doi.org/10.1016/j.ijmactools.2011.02.009>
- M.K. Gupta, Q. Song, Z. Liu, M. Sarikaya, M. Jamil, M. Mia, N. Khanna, G.M. Krolczyk, Experimental characterisation of the performance of hybrid cryo-lubrication assisted turning of Ti-6Al-4V alloy. *Tribol. Int.* **153**, 106582 (2021). <https://doi.org/10.1016/j.triboint.2020.106582>
- M. Perçin, K. Aslantas, I. Uçun, Y. Kaynak, A. Çicek, Microdrilling of Ti-6Al-4V alloy: the effects of cooling/lubricating. *Precis. Eng.* **45**, 450–462 (2016). <https://doi.org/10.1016/j.precisioneng.2016.02.015>
- S. Dinesh, V. Senthilkumar, P. Asokan, D. Arulkirubakaran, Effect of cryogenic cooling on machinability and surface quality of biodegradable ZK60 Mg alloy. *JMADE.* **87**, 1030–1036 (2015). <https://doi.org/10.1016/j.matdes.2015.08.099>
- S. Shukla, V. Bajpai, Effect of cryogenic quenching on microstructure and microhardness of Ti-6Al-4V alloy. *Mater. Lett.* **267**, 127532 (2020). <https://doi.org/10.1016/j.matlet.2020.127532>
- J.W. Won, J.H. Lee, J.S. Jeong, S.W. Choi, D.J. Lee, J.K. Hong, Y.T. Hyun, High strength and ductility of pure titanium via twin-structure control using cryogenic deformation. *Scr. Mater.* **178**, 94–98 (2020). <https://doi.org/10.1016/j.scriptamat.2019.11.009>
- L.S. Ahmed, N. Govindaraju, M.P. Kumar, L.S. Ahmed, N. Govindaraju, M.P. Kumar, Experimental investigations on cryogenic cooling in the drilling of titanium alloy experimental investigations on cryogenic cooling in the drilling of titanium alloy. *LMMP.* **31**, 603–607 (2016). <https://doi.org/10.1080/10426914.2015.1019127>
- A. Bagherzadeh, E. Budak, Investigation of machinability in turning of difficult-to-cut materials using a new cryogenic cooling approach. *Tribol. Int.* **119**, 510–520 (2018). <https://doi.org/10.1016/j.triboint.2017.11.033>
- M. Dhananchezian, M. Pradeep Kumar, Cryogenic turning of the Ti-6Al-4V alloy with modified cutting tool inserts. *Cryogenics (Guildf.)* **51**, 34–40 (2011). <https://doi.org/10.1016/j.cryogenics.2010.10.011>
- S.Y. Hong, Y. Ding, Cooling approaches and cutting temperatures in cryogenic machining of Ti-6Al-4V. *Int. J. Mach. Tools Manuf.* **41**, 1417–1437 (2001)
- D.B. Trivedi, J. Vasavada, S.S. Joshi, Microstructural assessment of drilled cross-sections on titanium generated under different cooling strategies. *Mater. Today Commun.* **26**, 101954 (2021). <https://doi.org/10.1016/j.mtcomm.2020.101954>
- A. Thakur, S. Gangopadhyay, State-of-the-art in surface integrity in machining of nickel-based super alloys. *Int. J. Mach. Tools Manuf.* **100**, 25–54 (2016). <https://doi.org/10.1016/j.ijmactools.2015.10.001>
- A. Shokrani, V. Dhokia, S.T. Newman, State-of-the-art cryogenic machining and processing. *Int. J. Comput. Integr. Manuf.* (2016). <https://doi.org/10.1080/0951192X.2012.749531>
- S. Basavarajappa, G. Chandramohan, M. Prabu, K. Mukund, M. Ashwin, Drilling of hybrid metal matrix composites-Workpiece surface integrity. *Int. J. Mach. Tools Manuf.* **47**, 92–96 (2007). <https://doi.org/10.1016/j.ijmactools.2006.02.008>
- F.J. Humphreys, M. Materials, S. Centre, Grain and subgrain characterisation by electron backscatter diffraction. *J. Mater. Sci.* **6**, 3833–3854 (2001)

26. S.K. Mishra, S.S.V. Tatiparti, S.M. Tiwari, R.S. Raghavan, J.E. Carsley, J. Li, Annealing response of AA5182 deformed in plane strain and equibiaxial strain paths. *Philos. Mag.* **93**, 2613–2629 (2013). <https://doi.org/10.1080/14786435.2013.781696>
27. J. Wu, P.J. Wray, C.I. Garcia, M. Hua, A.J. Deardo, Image quality analysis: A new method of characterizing microstructures. *ISIJ Int.* **45**, 254–262 (2005). <https://doi.org/10.2355/isijinternational.45.254>
28. M. Winking, G. Gottstein, L.S. Shvindlerman, Stress induced grain boundary motion. *Acta Mater.* **49**, 211–219 (2001). [https://doi.org/10.1016/S1359-6454\(00\)00321-9](https://doi.org/10.1016/S1359-6454(00)00321-9)
29. J. Dai, J. Xia, L. Chai, K.L. Murty, N. Guo, M.R. Daymond, Correlation of microstructural, textural characteristics and hardness of Ti–6Al–4V sheet β -cooled at different rates. *J. Mater. Sci.* **55**, 8346–8362 (2020). <https://doi.org/10.1007/s10853-020-04603-9>
30. H. Li, E. Hsu, J. Szpunar, H. Utsunomiya, T. Sakai, Deformation mechanism and texture and microstructure evolution during high-speed rolling of AZ31B Mg sheets. *J. Mater. Sci.* **43**, 7148–7156 (2008). <https://doi.org/10.1007/s10853-008-3021-3>
31. Z. Pu, J.C. Outeiro, A.C. Batista, O.W. Dillon, D.A. Puleo, I.S. Jawahir, Enhanced surface integrity of AZ31B Mg alloy by cryogenic machining towards improved functional performance of machined components. *Int. J. Mach. Tools Manuf.* **56**, 17–27 (2012). <https://doi.org/10.1016/j.ijmactools.2011.12.006>

Publisher's Note Springer Nature remains neutral with regard to jurisdictional claims in published maps and institutional affiliations.

Springer Nature or its licensor (e.g. a society or other partner) holds exclusive rights to this article under a publishing agreement with the author(s) or other rightsholder(s); author self-archiving of the accepted manuscript version of this article is solely governed by the terms of such publishing agreement and applicable law.